Research Article | Vol. 30, No. 14 / 4 Jul 2022 / Optics Express 24773

Optics EXPRESS

Interface engineering enhanced near-infrared electroluminescence in an n-ZnO microwire/p-GaAs heterojunction

JITAO LI,[1] BINGHUI LI,[2,4] MING MENG,[1] LINGLING SUN,[1] AND MINGMING JIANG[3,5]

[1]School of Physics and Telecommunications Engineering, Zhoukou Normal University, Zhoukou 466001, China
[2]State Key Laboratory of Luminescence and Applications, Changchun Institute of Optics Fine Mechanics and Physics, Chinese Academy of Sciences, Changchun 130033, China
[3]College of Physics, MIIT Key Laboratory of Aerospace Information Materials and Physics, Key Laboratory for Intelligent Nano Materials and Devices, Nanjing University of Aeronautics and Astronautics, No. 29 Jiangjun Road, Nanjing 211106, China
[4]binghuili@163.com
[5]mmjiang@nuaa.edu.cn

Abstract: Interface engineering in the fabrication of low-dimensional optoelectronic devices has been highlighted in recent decades to enhance device characteristics such as reducing leakage current, optimizing charge transport, and modulating the energy-band structure. In this paper, we report a dielectric interface approach to realize one-dimensional (1D) wire near-infrared light-emitting devices with high brightness and enhanced emission efficiency. The light-emitting diode is composed of a zinc oxide microwire covered by a silver nanolayer (Ag@ZnO MW), magnesium oxide (MgO) buffer layer, and p-type gallium arsenide (GaAs) substrate. In the device structure, the insertion of a MgO dielectric layer in the n-ZnO MW/p-GaAs heterojunction can be used to modulate the device features, such as changing the charge transport properties, reducing the leakage current and engineering the band alignment. Furthermore, the cladding of the Ag nanolayer on the ZnO MW can optimize the junction interface quality, thus reducing the turn-on voltage and increasing the current injection and electroluminescence (EL) efficiency. The combination of MgO buffer layer and Ag nanolayer cladding can be utilized to achieve modulating the carrier recombination path, interfacial engineering of heterojunction with optimized band alignment and electronic structure in these carefully designed emission devices. Besides, the enhanced near-infrared EL and improved physical contact were also obtained. The study of current transport modulation and energy-band engineering proposes an original and efficient route for improving the device performances of 1D wire-type heterojunction light sources.

1. Introduction

Near-infrared lighting sources, especially for the low-dimensional light-emitting diodes (LEDs) and laser diodes (LDs), have attracted increasing research interest in widespread applications, such as bioscience and biotechnology, night vision, surveillance, optical communications, etc [1–6]. For the last few years, low-dimensional near-infrared LEDs and LDs that showing high-performance and high-brightness have been illustrated experimentally, and those emission devices have been commonly fabricated based on narrow-bandgap semiconductors, low-dimensional organics nanocrystals, perovskites quantum dots, transitional metal doped fluorescent materials and so on [7–11]. Nevertheless, developing low-dimensional near-infrared light sources is currently restricted either by obviously lower stability and lower luminous efficiency, or much more disorganized and incomplete emission spectrum [12–14]. To address these problems, extensive efforts, including original physical mechanisms, new materials systems and novel device

#459837 https://doi.org/10.1364/OE.459837
Journal © 2022 Received 30 Mar 2022; revised 9 Jun 2022; accepted 15 Jun 2022; published 24 Jun 2022

structures, have been made to fabricate performance-enhanced near-infrared LEDs and LDs [15–18]. Generally, near-infrared light sources are primarily made of epitaxial heterostructures of III–V narrow-band inorganic semiconductors, such as GaAs, InP, InSb, GaAsAl, and so on, and these inorganic semiconductors have been provided powerful candidates in the design and development of near-infrared optoelectronic devices [7,19,20]. However, the fabrication of low-dimensional near-infrared light sources on account of narrow-band semiconductor micro/nanostructures has undergone a significant progress but requires complicated and expensive epitaxial preparation equipment, complex processing before/after growth, and the fabrication procedure is time-consuming [21–24].

Of late years, single crystal gallium arsenide (GaAs) is still the cornerstone of the modern electronic and information industry, and has asserted its dominance in large-scale device integration. Especially, the p-type GaAs film has been recognized as substantial platform for the application of low-dimensional heterojunction optoelectronic devices featuring in the near-infrared regions [25–27]. While, zinc oxide (ZnO), a direct wide-bandgap semiconductor (bandgap ~ 3.37 eV, exciton binding energy ~ 60 meV) that having high carrier mobility, high thermal and chemical stability, has been extensively utilized to construct wavelength-tunable light sources featuring in a wide range of wavelength band, including near-infrared, visible and ultraviolet regions [28–32]. Alternatively, by combining with p-type GaAs material, ZnO micro/nanostructures heterojunction based near-infrared light sources could be obtained by tailoring the electronic structure and controlling the carrier recombination path in a carefully designed ZnO/GaAs heterostructure. The combination of the merits of both the materials would make as-designed n-ZnO/p-GaAs heterojunction near-infrared light-emitter technically and practically competitive [33–37]. However, the device performances are greatly influenced by the current injection and confinement, discontinuous bandgaps, abundant interface states, intrinsic carrier mobility and contact resistance in the as-designed low-dimensional heterostructured optoelectronic devices [38–41].

In the present study, we report a kind of near-infrared LED, which is made of a ZnO microwire (MW) and p-type GaAs layer employing as its hole supplier. The LED exhibits a broadband light emission positioning at around 883.0 nm, and a spectral line-width ~ 65.5 nm. Nevertheless, the injection current-dependent evolution of the EL emissions was observed, suggesting the instability of fabricated device. To improve the LED performances, a dielectric MgO interlayer working as an electron blocking layer was inserted into the fabricated n-ZnO MW/p-GaAs heterojunction LED, which can suppress radiative recombination in the p-type GaAs layer, thus yielding a strong and stable near-infrared EL emissions occurring toward the heterointerface. Apart from the promising results, some unfavorable disadvantages for the insertion of MgO nanolayer in the as-constructed n-ZnO/p-GaAs heterojunction should be noticed, for instance, lower current injection, larger contact resistance, larger turn-on voltage and lower emission efficiency. To tackle these dilemmas, capping with Ag nanolayer on the wires can facilitate the carrier transport in the as-designed LEDs, and also make the electrical contact between ZnO MW and GaAs layer much more facilely and reliably, yielding performance-enhanced near-infrared LEDs. The resultant near-infrared EL features of the designed n-Ag@ZnO MW/MgO/p-GaAs heterojunction LEDs that having superiorities of low-cost and facile fabrication, can enable a constructive and prospective candidate with prospect of developing high-performance and high-brightness LEDs based on nanostructured semicondctors.

2. Experimental section

2.1. ZnO MWs synthesis

The growth of individual ZnO wires was accomplished by using a chemical vapor deposition (CVD) method. The uniform source materials were made up of highly-puritied ZnO and graphite (C) powders [33,35,42]. A quartz boat with the size of 4 cm (length) × 3.5 cm (width) × 2.0 cm (depth) was utilized to place the precursor mixture. A Si chip (the size of 3.5 cm (length) × 2.5 cm (width)) without any catalyst was placed on the quartz boat above the source materials with a vertical distance of about 1.55 cm. In the growth regime, the quartz boat was positioned at the heating area of a quartz tube in a horizontal tube electric furnace. A mixture of high-purity Ar including 5.0% O_2 was flowing into the furnace chamber at a total flow rate of 125 sccm. Before the furnace cooled down to room-temperature naturally, the temperature of the reactants regions was kept at 1050 °C for one hour. Finally, individual ZnO samples were obtained on Si substrate. The size of the as-grown ZnO wires could be controlled by manipulating the preparation condition, such as the precursor mixtures, growth time, growth temperature and carrier gas. The length can readily reach up to 2.0 cm, and the diameter varies from 0.5 to 80 μm.

To improve the optical and electrical properties of a ZnO MW, Ag nanolayer was introduced to deposite on the wire. The preparation procedure is summarized as follows: (i) a single ZnO MW was placed on a clean glass slide, immobilised with a indium (In) particles; (ii) ultra-pure Ag was evaporated on the MW using electron beam heating evaporation. Increasing the evaporating time can increase the thickness of Ag nanolayer, which evaporated on ZnO MWs [28,38,43].

2.2. Devices fabrication

A near-infrared light-emitting device, which is composed of an individual ZnO MW and p-type GaAs substrate, was designed. In the device structure, the commercially purchased p-type GaAs chip was employed as hole transporting source [32,33]. Briefly, the fabrication procedure of the device is following: (1) Ti/Au ohmic contact (30/40 nm) was first evaporated on an activated p-type GaAs layer utilizing electron beam heating evaporation; (2) MgO films with the thickness of about 5 μm were deposited onto the GaAs film using electron beam heating evaporation via a shadow mask; (3) An individual ZnO MW was mechanically transferred to place on p-GaAs film, with the pre-deposited MgO films located along both the sides of the wire; (4) Finally, the ITO conductive glass was bonding with MW inversely and acted as the top ohmic contact electrode of the n-ZnO MW/p-GaAs heterojunction device. Thus, the MgO films deposited on bilateral sides of the GaAs film can work as insulating layers to prevent the direct contacting between ITO top electrode and p-GaAs film. A typical device configuration of the designed n-ZnO MW/p-GaAs heterojunction is depicted in Fig. 2(a).

To engineering the band alignment of n-ZnO MW/p-GaAs heterojunction, a dielectric MgO interlayer with the thickness of about 10 nm was evaporated on the p-type GaAs film by using electron beam heating evaporation. Schematic of the complete structure of the as-designed n-ZnO MW/MgO/p-GaAs heterojunction LED is shown in Fig. 4(a) [36,39]. Besides, using electron beam heating evaporation, Ag nanolayer with 15 nm in thickness was evaporated on ZnO MW. Accordingly, the schematic illustration of the fabricated n-Ag@ZnO MW/MgO/p-GaAs heterojunction LED is further shown in Fig. 4(e) [44,45].

2.3. Device characterization

A Keysight B1500A sourcemeter system is used to measure the electrical characterization via current-voltage (I-V) curves of ZnO samples, p-GaAs chip and the fabricated single MW heterojunction emission devices. Optical properties of the as-synthesized ZnO samples and GaAs chip were measured using a photoluminescence (PL) system at room temperature with a 325 nm He-Cd laser via a high-resolution LabRAM-UV Jobin-Yvon spectrometer and a high-sensitivity charge-coupled device (CCD). EL measurement of the as-fabricated heterojunction device was carried out using a microspectral detection system, which is made of a ANDOR detector (CCD-13448) and Omni-λ 500 Spectrograph. An optical microscope was used to collect the EL images of the as-fabricated heterojunction light sources via a CCD camera. In the EL characterization, a direct and continuous current power source was utilized to bias the fabricated emission devices. All the experimentals were performed at room temperature.

3. Results and discussions

The ZnO wires investigated in this work were characterized [33,35]. The structural characterization of ZnO samples, containing microscopic structure, surface morphology and topography, was viewed by using a scanning electron microscope (SEM). Shown in Fig. 1(a), hexagon-shaped cross-sectional profile of a ZnO MW is obtained, and the cross-sectional size of the wire is measured to approximately 15 μm. Thus, individual ZnO wires with hexagon-shaped profiles and well-defined facets, were successfully prepared. The phase and purity of the as-synthesized ZnO wires were characterized by powder X-ray diffraction (XRD). The XRD result shown in Fig. 1(b) exhibits a strongest (100) peak located at 31.7°, confirming that the as-grown ZnO MWs have a relatively good c-axis preferred orientation, and typical wurtzite crystal structure [28,44]. Further, it is observed that the full width at half maximum (FWHM) of the sharp peak in the XRD pattern (100) is extracted to about 0.065°, suggesting that the as-synthesized ZnO samples possess the high-crystalline nature [45,46].

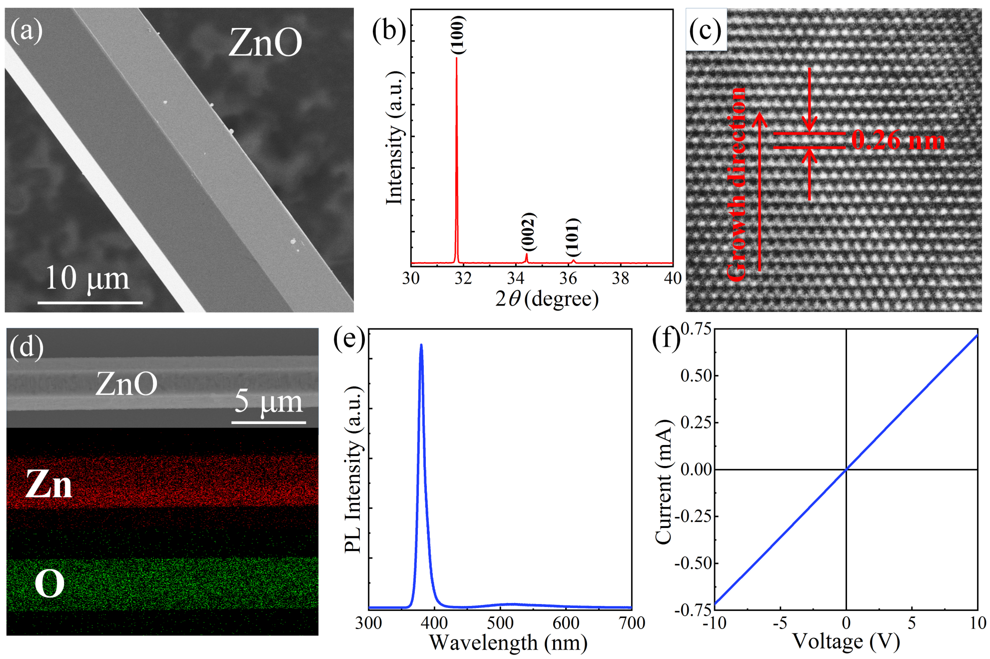

Fig. 1. (a) SEM image of a ZnO MW, and the diamter is evaluated to about 15 μm. (b) XRD result of the as-synthesized ZnO samples. (c) HRTEM picture of a ZnO wire. (d) Image of a ZnO MW and corresponding Zn and O elemental maps. (e) PL result of a ZnO MW. (f) *I-V* characteristic curve of an individual ZnO MW, with In particles serving as electrodes.

The as-synthesized ZnO wires were further analyzed by utilizing transmission electron microscopy (TEM). The regular lattices of typical wurtzite crystal structure is deterimined with an indication of high crystallinity within the as-grown ZnO sample. Its high-resolution TEM image was shown in Fig. 1(c), demonstrating a clear lattice fringe. The measured spacing between the crystal planes is around 0.26 nm, and the corresponding crystal plane is (100) [46]. The composition of a ZnO MW was determined by using energy-dispersive X-ray spectroscopy (EDS), indicating the presence of Zn and O elemental distribution, as illustrated in Fig. 1(d). The components of Zn and O appear evenly on a ZnO wire. Optical properties of a single ZnO MW was tested and the PL spectrum is shown in Fig. 1(e). The ZnO MW emits at the band-edge of ZnO (~ 380 nm) with a line width of about 12.0 nm, accompanying by an insignificant visible emission. The PL result suggests that the synthesized ZnO wires possess remarkably high crystalline quality [28,46]. Electrical property of a single ZnO MW was performed. The *I-V* characteristic curve illustration in Fig. 1(f), is closing to linear, indicating that the electrical contact between In electrode and ZnO wire formed a relatively good Ohmic property.

As we described in the Experimental Section, a kind of near-infrared emission device involving a single ZnO MW and p-type GaAs film, was fabricated. Figure 2(a) illustrates a schematic diagram of the n-ZnO MW/p-GaAs heterojunction light-emitting device. The p-type GaAs layer is employed as the hole supplier in the device architecture. A Keysight B1500A sourcemeter system was employed to measure electrical transport characteristics of the as-constructed single MW heterojunction device, operating at room temperature. First, electrical characterization of the p-type GaAs film was performed, with Ti/Au films worked as electrodes. Good Ohmic contact between the Ti/Au electrode and p-type GaAs film is determined by the linear behavior, as shown in Fig. 2(b) [38,44].

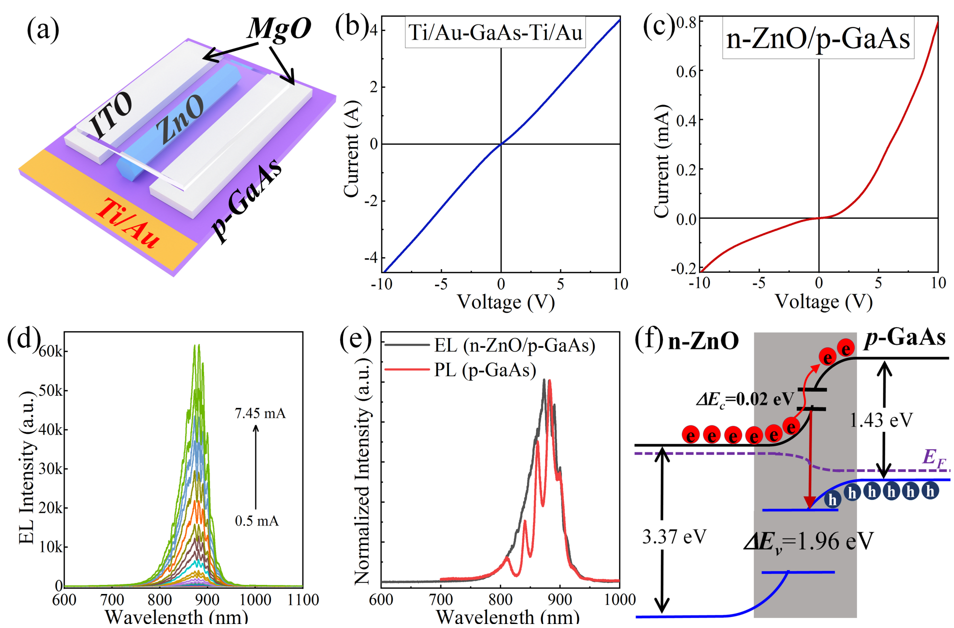

Fig. 2. Device characterization of the fabricated n-ZnO MW/p-GaAs heterojunction near-infrared LED. (a) Schematic of a heterojunction emission device, containing a ZnO MW and p-type GaAs substrate. In the LED configuration, ITO conducting glass and Ti/Au nanolayer featuring as electrodes for the carriers injection. (b) *I-V* characteristic curve of p-type GaAs substrate, with Ti/Au nanolayers serving as electrodes, forming Ohmic contact. (c) *I-V* curve of the fabricated n-ZnO MW/p-GaAs heterostructure, suggesting diode-like rectifying characteristic. (d) EL spectra with increasing current injection in the range of 0.5 to 7.45 mA at room temperature. (e) Normalized PL spectrum of GaAs substrate, and normalized EL spectrum of as-fabricated n-ZnO MW/p-GaAs heterojunction LED at the input current ~ 5.0 mA. (f) Schematic diagram of the energy band configuration of n-ZnO MW/p-GaAs heterojunction LED.

Electronic transport property of the as-constructed n-ZnO MW/p-GaAs heterojunction device was performed. As depicted in Fig. 2(c), LED-like rectifying behavior is acquired in the n-ZnO/p-GaAs heterojunction. As we demonstrated above, the contacting characters between the ZnO MW and In is assigned to Ohmic contact, which was examined by inputting a current through the In-ZnO-In structure (Two In particles were fixed at the ends of the MW, working as electrodes). Because of the good Ohmic contacts for Ti/Au electrode on GaAs film and In-ZnO, the rectifying behavior characteristic should be ascribed to the p-n heterojunction formed between n-ZnO MW and p-GaAs film [35,37,47]. The turn-on voltage of the device is examined to around 1.25 V. As the applied forward bias increasing, the I-V curve of the device become much steeper and the current rise more rapidly. But it is regrettable that the reverse leakage current of the as-fabricated heterojunction device was evaluated to about 0.21 mA at a reverse bias of -10 V, yielding much larger leakage current. It may be caused by surface defects or trap-center concentration at the interface of n-ZnO MW/p-GaAs [37].

In forward bias, the EL characterization of fabricated n-ZnO MW/p-GaAs heterojunction optoelectronic devices was performed at room temperature (As described in Experimental Section). When the forward bias increasing above the turn-on voltage, near-infrared light-emission can be observed. The light signals were detected using a spectrometer. Illustration in Fig. 2(d) are the EL spectra of the as-fabricated n-ZnO MW/p-GaAs heterojunction LED, which were measured by varying the injection current in the range of 0.5–7.45 mA. The device emits near-infrared light-emission peaking at around 883.0 nm under various forward injection current, and the spectral line width is measured to about 65.5 nm. The integrated EL intensity increased almost linearly by increasing the input current. Besides, the main peak position illustrated a slight blue shift varying from 895.6 to 880.3 nm. And the blueshifted phenomenon could be attributed to the variation of radiative recombination regions. When a forward voltage was applied on the as-constructed n-ZnO MW/p-GaAs heterojunction, large quantities of electrons and holes would be injected into the heterojunction, but the subsequent recombination process might be accomplished via different transition paths: (i) one of the recombination process may occur at the p-type GaAs template, originating from the band-edge emission of GaAs material; (ii) while the other light-emission should originate from the carrier recombination across the band offset at the depletion region of n-ZnO/p-GaAs heterointerface [37,44,47]. Therefore, the minior band offset may give rise to a more complex recombination likelihood due to the principle of quantum transition.

Normalized PL result of p-GaAs layer and EL result of the as-fabricated n-ZnO MW/p-GaAs heterojunction LED is given in Fig. 2(e) for a comparison. Shown in the figure (the red solid line), the peak emission wavelength of GaAs film positioned at around 882.0 nm under the irradiation of an ultraviolet source (He-Cd laser ~ 325 nm), which was usually attributed to the band-edge emission of GaAs material [7,12]. The corresponding line width is checked to about 40 nm, which is spectrally narrower than that of the EL spectrum obtained of the as-constructed n-ZnO MW/p-GaAs heterojunction LED. Comparing with the PL emissions of ZnO MW and GaAs film, the main EL peak energy is not identified with either the typical NBE emission, or the much weaker visible emission of ZnO MW. Nevertheless, the PL profile of GaAs film matched with the main EL peaks of the as-fabricated n-ZnO MW/p-GaAs heterojunction LED [37,47]. In addition, both PL and EL spectra showed asymmetric shape, which was usually attributed to the band-filling effect, causing the bulk Fermi level shift to a higher position within the conduction band. Therefore, the much broad near-infrared emission band obtained in the as-fabricated heterojunction LED could be attributed to the superposition of the band-edge of GaAs film, and carrier radiative recombination across the band offset at the depletion region of n-ZnO/p-GaAs [33,35,36].

To further investigate the working principle of current transport and EL emission, the energy band structure diagram of the n-ZnO MW/p-GaAs heterojunction was designed. The electron affinities ψ of ZnO and GaAs are $\psi_{ZnO} \sim 4.35$ and $\psi_{GaAs} \sim 4.07$ eV, respectively. The energy bandgaps of ZnO (E_{ZnO}) and GaAs (E_{GaAs}) are ~ 3.37 and ~ 1.43 eV, respectively [33,35]. When the heterojunction between ZnO MW and p-type GaAs was formed, a band discontinuity would occur at the interface. Notably, a typical staggered type-II heterojunction will be constructed between the ZnO MW and p-type GaAs. Under thermal equilibrium at 0 V, the barrier height at

Optics EXPRESS

the interface for the conduction bands and valence bands, ΔE_c and ΔE_v, were derived to be ~ 0.02 eV and ~ 1.96 eV, respectively. Under such a heterojunction configuration, the band offset between n-ZnO MW and p-GaAs layer is calculated to about 1.41 eV. As illustrated in Fig. 2(f), when a forward voltage was applied on the as-constructed n-ZnO MW/p-GaAs heterojunction device, large quantities of electrons and holes would be injected into the heterojunction [37]. The energy band of ZnO would bend upward in the contacting region, which is adjacent to the ZnO/GaAs interface. And the larger barrier height at valence bands between ZnO and GaAs would prevent the holes in the p-type GaAs layer moving to the ZnO MW [33,35]. Nevertheless, the electrons injected into ZnO MW could diffuse to the p-GaAs side under higher forward bias, which is due to the much smaller barrier at the n-ZnO/p-GaAs interface for the conduction bands [39,44,45]. In this case, the radiative recombination would be favored to occur across the band offset at the depletion region of n-ZnO/p-GaAs, as well as in the p-type GaAs side. Consequently, the broad near-infrared light-emission observed in the EL spectra should be originated from the carrier recombination across the band offset at the depletion region of n-ZnO/p-GaAs, and the p-type GaAs materials [37].

Details on the near-infrared EL characterization of the as-fabricated LED was further tested. Luminescence photos of near-infrared EL were captured, and illustrated in Fig. 3(a) and 3(b). As the applied bias beyond the turn-on voltage, the device begins to emit near-infrared light emission, and the light-emitting areas situated at the sharp edges of the hexagon-shaped wires. Its brightness and illuminating regions increase monotonously by increasing the operating currents. Besides, the dark region observed along the wire was originated from the nonuniform electronic contact at the n-ZnO MW/p-GaAs interface. Combining with p-GaAs layer, ZnO micro/nanostructures can be used to developing GaAs-based optoelectronic devices, featuring in the near-infrared wavelengths [33,35,37].

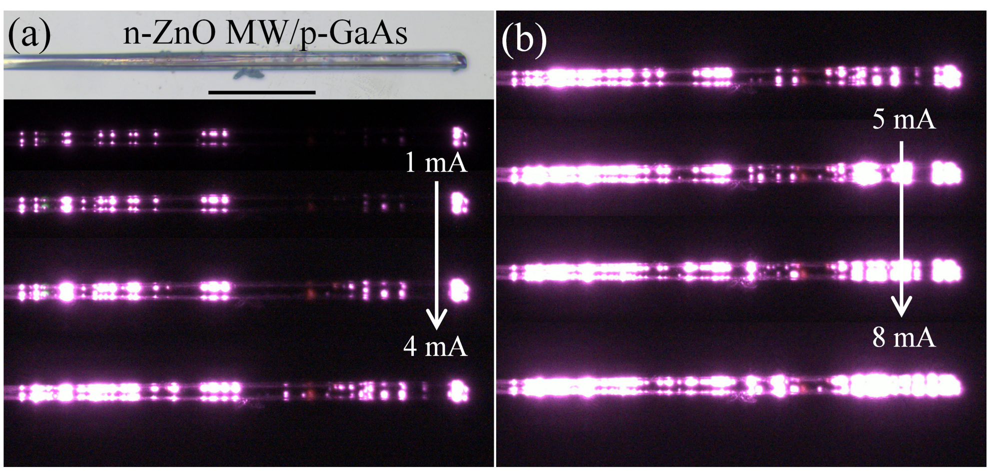

Fig. 3. Optical microscopic EL images of the designed LED were recorded using a CCD. (a) Optical microscopic EL images of the device by varying the injection current in the range of 1–4 mA. (b) Optical microscopic EL images by increasing the injection current in the range of 5–8 mA. The scale bar is 60 μm.

GaAs, as a promising material with a narrow band gap and excellent electrical characteristics, has been drawing much attention in the fields of photodetectors, LEDs and LDs working in the near-infrared wavelengths [7,25–27]. The attractiveness in fabricating low-dimensional GaAs-based optoelectronic devices has been hindered because of the expensive epitaxial growth equipment of preparing nano/microstructures [21,23,24]. Therefore, the combination of ZnO with various kinds of nano- and microstructures and p-type GaAs substrate, can provide an

Optics EXPRESS

alternative strategy for realizing long-wavelength, high-performance LEDs and LDs in the future [35,36]. However, the fabrication of low-dimensional n-ZnO/p-GaAs heterostructured optoelectronic devices suffers from several dilemmas: (1) much larger leakage current, which is caused by the smaller energy barrier of conduction band off-set at n-ZnO/p-GaAs interface and the higher electron mobility of ZnO, would deteriorate the EL performances in accelerating the efficiency-droop influence at high current levels; (2) the much low light-emission efficiency could be induced by the competition of carrier radiative recombination occuring in p-GaAs side and at the n-ZnO/p-GaAs interface; (3) nonuniform electronic contact between ZnO MW and GaAs layer in the case of ordinary, directly physical contact [37,44,47].

Substantial attempts on interfacial optimization have been devoted to enhancing the LED performances. Referring to previous reports, the energy band alignment of heterojunction optoelectronic device can be engineered by introducing a dielectric buffer layer. To manipulate the current injection route, MgO layer working as electron blocking layer would be inserted into the as-designed n-ZnO MW/p-GaAs heterojunction emission device [39,44,48]. Schematic illustration of the fabricated device is shown in Fig. 4(a). The effect of MgO layer on the carrier transport modulation is illustrated in Fig. 4(b) in terms of the band alignment. According to the electron affinities of ZnO, MgO and GaAs, the conduction-band offset between ZnO and MgO is evaluated to about 3.55 eV [34,39]. Under the forward bias, the injected electrons will be restrained and accumulated in the quasi-Fermi levels (E_{fn}) at the side of ZnO MW. The valence-band offset $\sim \Delta E_v$ is estimated to about 2.0 eV, producing a band discontinuity at the interface. The injected holes could be accumulated in the quasi-Fermi levels (E_{fp}) at the side of GaAs film [37]. In the case of the as-constructed n-ZnO MW/MgO/p-GaAs heterojunction, the reverse current would be dramatically suppressed due to the insertion of MgO layer, which would be discussed below [34,44]. However, the turn-on voltage of the single MW heterojunction with MgO interlayer device is larger than that of the device structure at the absence of MgO layer; and the electrical transport properties of the device became poorer because of the bigger series resistance of the MgO electron blocking layer [34,39,44].

To improve the LED characteristics of the as-constructed n-ZnO MW/MgO/p-GaAs heterojunction device, the strategy is introducing Ag nanolayer with the thickness of about 15 nm to cover ZnO MW. The optical and electrical properties of a single ZnO MW uncovered and covered by Ag nanofilms were characterized. Figure 4(c) exhibits a SEM observation of a bare ZnO MW. While introducing Ag nanofilm decoration, the surface morphology was further viewed and displayed in Fig. 4(d). Thus, Ag nanofilms with desired thickness can be evaporated on the wires. The PL properties of a single ZnO MW not covered and covered by Ag nanolayer was measured, and the corresponding PL spectra are depicted in Fig. 4(e). It is indicated that a clear enhancement of typical near-band emission of ZnO MW is obtained. While, the visible emission is observably suppressed by using the cladding of Ag nanolayer (Shown in Fig. 4(f)) [43,49]. Thus, the cladding Ag nanofilms on ZnO MW can act as protective capping and surface passivation. The treatment of capping with a 15 nm Ag nanofilms is a useful method to enhance the optical properties of a ZnO MW, including near-band edge emission enhancement and a significant suppression of its visible emission. It declares that obvious number of surface traps were successfully removed. The PL enhancement in a single ZnO MW covered by Ag nanofilms can be attributed to the cooperative influences of outer surface cleaning modulation, the reduction of non-radiative recombination centers and the increased neutral donor levels [50,51].

Meanwhile, the *I-V* curves of a single ZnO MW not decorated and decorated by Ag nanolayer were plotted in Fig. 4(g). The linear behavior suggests that the contact between the ZnO MW uncovered and covered by Ag nanofilms can form an ohmic contacting features by using In electrode [28,52]. Previous literature reported that surface conditions of ZnO nano- and microstructures play a crucial role on current transport across the metal-semiconductor interface. The strong dependence represented that the underlying factors, for instances the surface states,

Optics EXPRESS

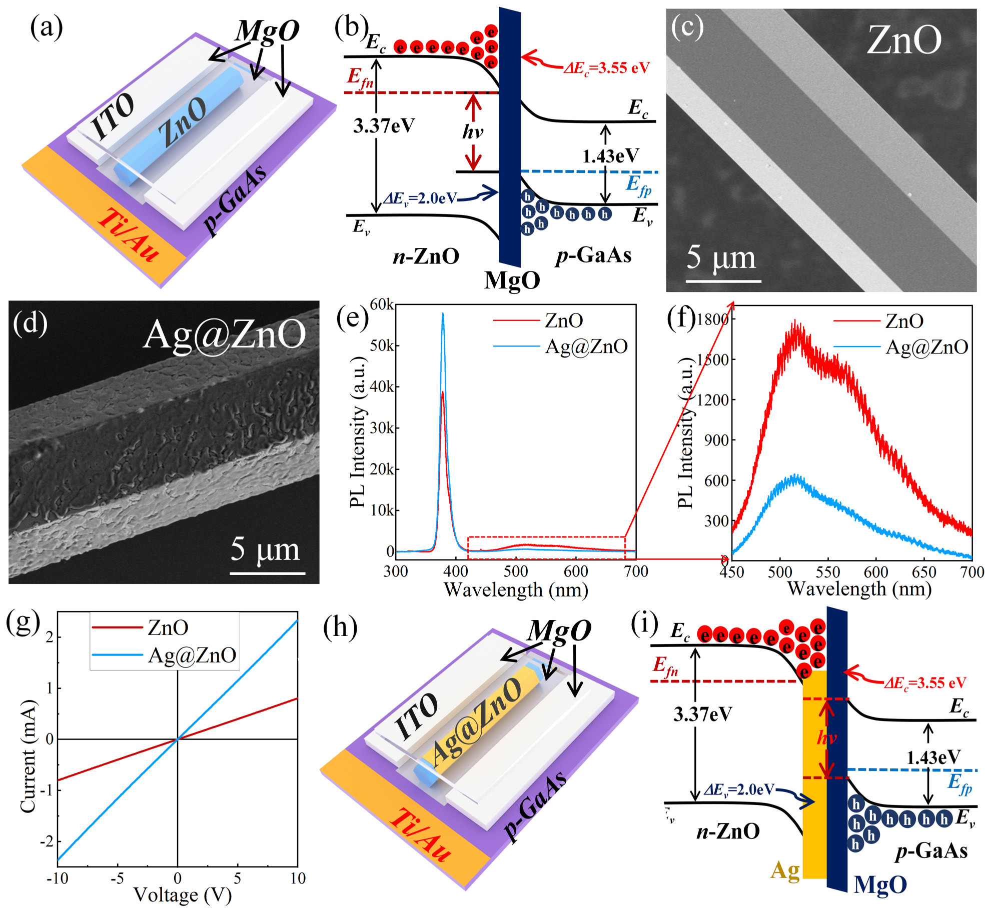

Fig. 4. (a) The schematic diagram of a single MW heterojunction LED, containing a ZnO MW, MgO insulating layer and p-type GaAs substrate. In the LED configuration, ITO conducting glass and Ti/Au nanolayer featuring as electrodes for the current injection. (b) Energy band structure of the as-constructed n-ZnO MW/MgO/p-GaAs heterojunction LED under forward bias. (c) A SEM image of a bare ZnO MW. (d) A SEM image of the ZnO MW covered by Ag nanofilm. (e) PL results of a single ZnO MW not covered and covered by Ag nanolayer. (f) The enlarged PL spectra, which is marked in (e), featuring in the visible band. (g) *I-V* curves of a single ZnO MW not covered and covered by Ag nanolayer. (h) The diagrammatic diagram of the as-constructed single MW heterojunction device structure, containing a ZnO MW covered by Ag nanolayer, a MgO nanolayer and p-type GaAs substrate. (i) Energy band structure of the as-constructed n-Ag@ZnO MW/MgO/p-GaAs heterojunction LED under forward bias.

Optics EXPRESS

crystal quality and surface treatment have a distinct modulation on ZnO barrier heights as opposed to adjust the ranges of barrier heights, which could be typically attributed to Fermi level pinning or metal-induced gap states at other semiconductor contacts [29,53,54]. Because of the relatively higher crystal quality of the as-synthesized ZnO MWs, the localized Schottky barrier formed between Ag and ZnO MW makes little influence on the current transport properties in a single ZnO MW. Conclusively, a distinct enhancement of electronic transport property observed in a single ZnO MW can be assigned to the surface treatment of capping Ag nanofilms [34,52,55].

Accordingly, a p-n heterojunction emission device, which is composed of a ZnO MW covered by Ag nanolayer, MgO nanolayer and p-GaAs substrate, was constructed. The device structure is schematically illustrated in Fig. 4(h). To study the mechanism of current transport and EL emission, the energy band structure diagram of the n-Ag@ZnO/MgO/p-GaAs heterojunction was designed, and shown in Fig. 4(i). As the work function of Ag ~ 4.26 eV is smaller than that of ZnO electron affinity (~ 4.35 eV). The capping Ag films has little modulation on the energy band alignment of the fabricated n-Ag@ZnO MW/MgO/p-GaAs heterojunction device. Under the nonequilibrium condition, the conduction band offset and the valence band offset between Ag@ZnO and GaAs is 3.55 and 2.0 eV, respectively. In the device structure, MgO, a low-dielectric material, with Ag together forms a stepped energy level structure between n-ZnO and p-GaAs. After inserting the Ag/MgO nanobuffer, electrons are blocked on the ZnO side (~ quasi-Fermi levels E_{fn}); while the injected hole are blocked on the GaAs side (~ quasi-Fermi levels E_{fp}), respectively [34,38,45].

Electrical characterization of the as-fabricated single MW heterojunction devices were measured. In the device architecture, the n-ZnO MW/MgO/p-GaAs heterojunction emission device is defined as ZnO&LED-1. By introducing Ag nanolayer deposited on the surface sides of the wire, the as-fabricated n-Ag@ZnO MW/MgO/p-GaAs heterojunction emission device is defined as Ag@ZnO&LED-2. The *I-V* curves of the measured ZnO&LED-1 and Ag@ZnO&LED-2 are shown in Fig. 5(a). The *I-V* results exhibit excellent rectifying diode-like behavior, yielding the heterostructured p-n junction of emission devices. The turn-on voltage of the ZnO&LED-1 device is extracted to about 6.3 V (red solid line). And, much lower leakage current of about 10^{-4} mA even at a reverse bias reaching 10 V. Specifically, by introducing Ag nanolayer deposited on the ZnO MW, the significantly improved electrical performance of the Ag@ZnO&LED-2 is achieved (Fig. 5(a), blue solid line). Apart from diode-like rectifying characteristics, the turn-on voltage of the as-fabricated n-Ag@ZnO MW/MgO/p-GaAs heterojunction LED was estimated to be 4.25 V, which is much smaller than of the ZnO&LED-1. It should be noted that, the electrical transport properties of the Ag@ZnO&LED-2 is observably increased than that of the ZnO&LED-1.

Under the operation of forward bias above the turn-on voltage, the light-emitting characterization of the as-fabricated LEDs were measured. Figure 5(b) exhibited EL spectra of the ZnO&LED-1 by varying the injection current in the range of 0.35–7.4 mA. The LED demonstrates typical near-infrared light-emission with the EL wavelengths peaking at around 875.5 nm, and the spectral linewidth of the EL spectra is extracted to about 55 nm. There is no significant shift in the emission peak position with increasing injection current, suggesting a small level of quantum-confined Stark-effect. By incorporating Ag nanolayer on the wire, EL spectra of the as-fabricated Ag@ZnO&LED-2 is plotted in Fig. 5(c), with the injection current ranging from 0.20 to 5.65 mA. Illustration in the EL spectra, a strong near-frared light-emission peaking at 872.5 nm is obtained. Similarly, no obvious variation in the main EL peak position could be observed with increasing injection current. The EL spectra from the same MW not covered and covered by Ag nanofilm at the same injection current of 5.5 mA, were plotted in Fig. 5(d). Compared with the LED that without Ag nanofilm cladding, a 5.5-fold increasement in EL intensity was obtained.

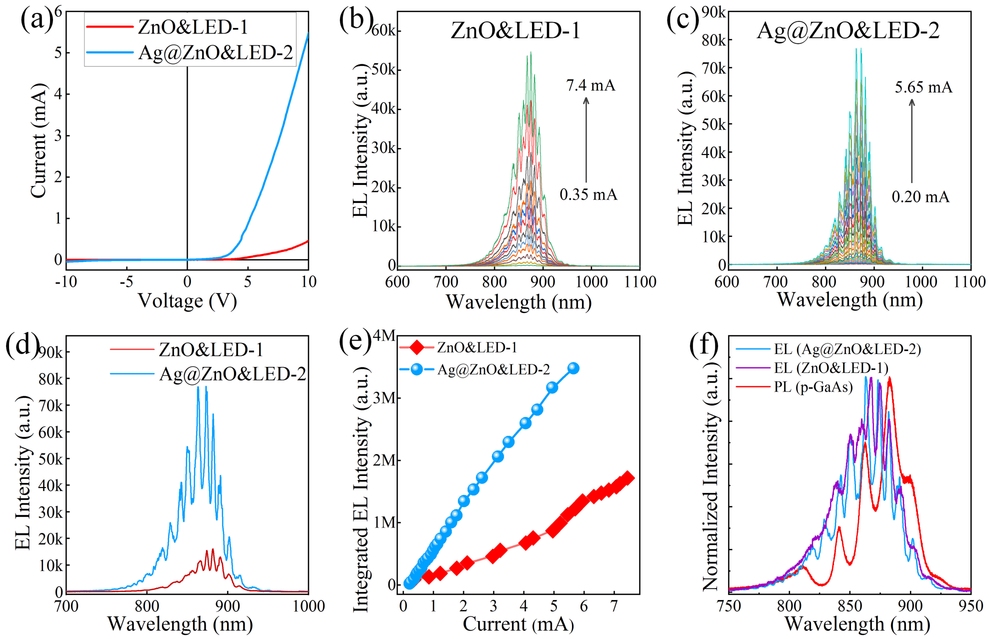

Fig. 5. LED characterizations. (a) *I*-*V* curves of the fabricated heterojunction devices. In the devices, the usage of ZnO MW is not covered, and covered by Ag nanolayer. The curves suggested diode-like rectifying characteristics. (b) EL spectra of the as-designed ZnO&LED-1 device with an increase of injection current ranging from 0.35 to 7.4 mA. (c) EL spectra of the as-designed Ag@ZnO&LED-2 device with increasing the injection current in the range of 0.2–6.65 mA. (d) Comparison of EL spectra of the as-fabricated single MW heterojunction LEDs. The injection current is 5.5 mA. (e) Comparisopn of integrated EL intensity versus different injection current. (f) Normalized PL spectrum of GaAs substrate, and normalized EL spectrum of as-fabricated n-Ag@ZnO MW/MgO/p-GaAs heterojunction LED at an input current ~ 5.0 mA.

Light–current characteristics of the as-fabricated LEDs were performed. Figure 5(e) illustrates the corresponding integrated EL intensities of the LED light sources versus various injection current. It is observably seen that the light intensity increases near-linearly by varying the injection current for the fabricated LEDs. By comparing with the ZnO&LED-1, the EL light intensity of the Ag@ZnO&LED-2 increases sharply with increasing the driving current. Thus, the incorporation of Ag nanofilm depositing on the ZnO MW can lead to a significant increase of the light-current of the fabricated LEDs. In addition to a little blueshift of the enveloped EL profiles, the significantly enhanced EL intensity is thus largely assigned to the cooperative consequence of the improved electrical performance of single Ag@ZnO MW, as well as the performance-optimized n-ZnO/MgO/p-GaAs heterojunction [45]. Consequently, the device performance and emission efficiency were dramatically enhanced, and the enhancement mechanism is ascribed to the effective current injection and optimized p-n junction.

The normalized EL spectra of the as-fabricated ZnO&LED-1 and Ag@ZnO&LED-2 at the same injection current of 5.5 mA were compared in Fig. 5(f) (the blue and violet solid lines), and the normalized PL spectrum of p-GaAs layer (the red solid line) was also shown in Fig. 5(f). As we described above, the EL spectra of as-fabricated ZnO&LED-1 and Ag@ZnO&LED-2 illustrated a slight blue shift. Thus, the EL emission occuring in the p-type GaAs side was significantly suppressed after inserting the MgO nanolayer. Besides, at the presence of the MgO nanolayer, the injected electrons will be restrained and accumulated in the ZnO MW, and the

Optics EXPRESS

carrier radiative recombination can occurr at the heterointerface between GaAs and ZnO MW, which is favorable to the high-efficiency near-infrared light-emission. Further, by covering Ag nanolayer on the wire, the EL efficiency can be increased observably. Therefore, we proposed a promising candidate to construct high-brightness and performance-enhanced near-infrared light-emission devices utilizing interface engineering of heterojunction with optimized band alignment and heteromicrostructures.

Under forward bias, optical images of the resulting LEDs were captured using a CCD digital camera via optical microscope objective. Figure 6(a) presents the optical microscope images of the ZnO&LED-1 by varying the injection current in the range of 3.0–5.0 mA. With the help of pseudocolor camera, we observe remarkably bright, near-infrared light emission from the single MW heterojunction LED. The light-emission regions are distributed along the wire, and its intensity is increased. Regrettably, the dark regions along the wires, which observed in the microscope EL images, were resulted from the nonuniform electronic contact at the interface. By incorporating Ag nanolayer on ZnO MW, significantly enhanced lighting brightness and emission regions of the Ag@ZnO&LED-2 can be obtained, and the corresponding optical microscope images are collected and shown in Fig. 6(b). In which, the injection current varied from 3.0 to 5.0 mA. Bright and near-infrared light-emission can be clearly seen from the as-fabricated Ag@ZnO&LED-2. The bright light-emission is observed clearly across the entire body of MW region and its intensity increased by increasing the injection current. It needs to be emphasized that, the dark regions captured in the Ag@ZnO&LED-2, were greatly reduced. It is envisioned that the incorporation of MgO electron blocking layer and Ag nanolayer with optimized design can be exploited to effectively engineering the barrier height of a heterogeneous semiconductor interface in case of n-ZnO MW/p-GaAs heterostructured emission devices, and can result in high-brightness LEDs with significantly increased performances [36,49].

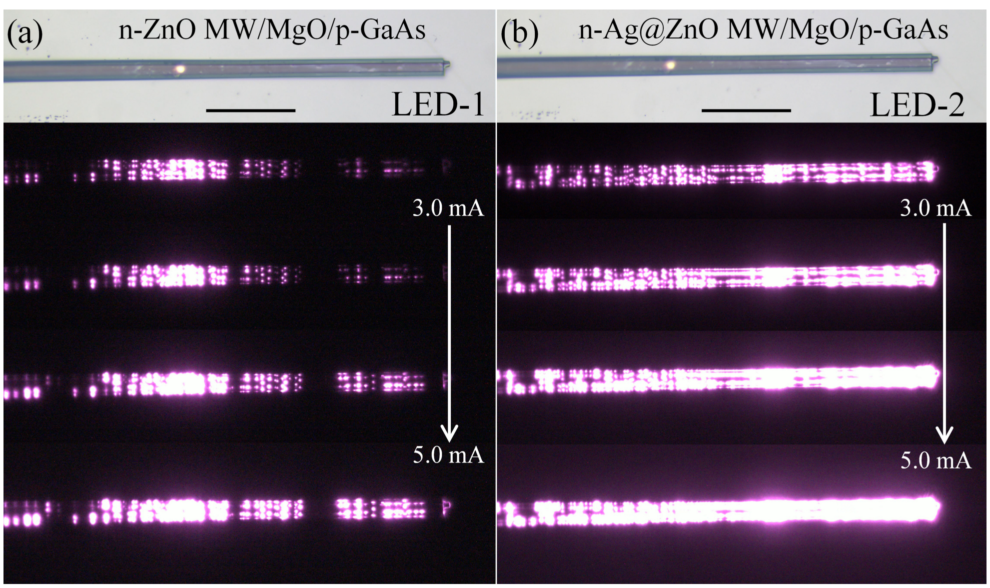

Fig. 6. Micrographs of near-infrared light emissions from single MW based LED as the applied bias above the turn-on voltage: (a) optical micrographic EL images of as-fabricated ZnO&LED-1 with the injection current in the range of 3.0–5.0 mA. The scale bar is 50 μm. (b) Optical micrographic EL images of as-fabricated Ag@ZnO&LED-2 device with various currents ranging from 3.0 to 5.0 mA. The scale bar is 50 μm.

4. Conclusion

In summary, we have proposed a workable approach to fabricate high-brightness and high-performance near-infrared light sources by constructing a n-Ag@ZnO MW/MgO/p-GaAs heterostructure. In the device architecture, a dielectric MgO layer was employed to engineering the energy band alignment of n-ZnO/p-GaAs heterojunction, together with a dramatic reduce of the device leakage current; Further, cladding Ag nanolayer on the ZnO MW is beneficial for further lowering the turn-on voltage, increasing current injection and passivating interfacial defects, thus increasing device EL efficiency. The working principle behind the performance-enhanced EL emissions of the as-designed LEDs is ascribed to tailoring energy-band alignment, enhancing electronic characteristics and modulating the carrier recombination path in a carefully designed n-ZnO MW/p-GaAs heterostructure. Although further optimizing the device structure, containing the carrier charge injection and transporting path, p-n junction performance and energy-band alignment, is still needed, the finding presented here supplies an alternative scheme to improve the near-infrared EL performances of n-ZnO structure/p-GaAs heterojunction emission devices.

Funding. Fundamental Research Funds for the Central Universities (NC2022008); National Natural Science Foundation of China (11874220, 11974182); the Science and Technology Development Plan Project of Henan Province (222300420597); Key Scientific Research Project of Colleges and Universities in Henan Province (22A140033).

Disclosures. The authors declare that there are no conflicts of interest related to this article.

Data availability. Data underlying the results presented in this paper are not publicly available at this time but may be obtained from the authors upon reasonable request.

References

1. M. Vasilopoulou, A. Fakharuddin, F. P. Garcia de Arquer, D. G. Georgiadou, H. Kim, A. R. b. Mohd Yusoff, F. Gao, M. K. Nazeeruddin, H. J. Bolink, and E. H. Sargent, "Advances in solution-processed near-infrared light-emitting diodes," Nat. Photonics **15**(9), 656–669 (2021).
2. Z. Chen and M. Segev, "Highlighting photonics: looking into the next decade," eLight **1**(1), 2 (2021).
3. X. Wu, Y. Zhang, K. Takle, O. Bilsel, Z. Li, H. Lee, Z. Zhang, D. Li, W. Fan, C. Duan, E. M. Chan, C. Lois, Y. Xiang, and G. Han, "Dye-sensitized core/active shell upconversion nanoparticles for optogenetics and bioimaging applications," ACS Nano **10**(1), 1060–1066 (2016).
4. Y. Gu, Z. Guo, W. Yuan, M. Kong, Y. Liu, Y. Liu, Y. Gao, W. Feng, F. Wang, J. Zhou, D. Jin, and F. Li, "High-sensitivity imaging of time-domain near-infrared light transducer," Nat. Photonics **13**(8), 525–531 (2019).
5. A. Minotto, P. A. Haigh, L. G. Lukasiewicz, E. Lunedei, D. T. Gryko, I. Darwazeh, and F. Cacialli, "Visible light communication with efficient far-red/near-infrared polymer light-emitting diodes," Light: Sci. Appl. **9**(1), 70 (2020).
6. Z. Lv, Z. Man, Z. Xu, C. Feng, Y. Yang, Q. Liao, X. Wang, L. Zheng, and H. Fu, "Intracellular near-infrared microlaser probes based on organic microsphere-SiO2 core-shell structures for cell tagging and tracking," ACS Appl. Mater. Interfaces **10**(39), 32981–32987 (2018).
7. H. Suchomel, M. Klaas, S. Betzold, P. Gagel, J. Beierlein, S. Klembt, C. Schneider, and S. Hofling, "Spatio-temporal coherence in vertically emitting GaAs-based electrically driven polariton lasers," Appl. Phys. Lett. **116**(17), 171103 (2020).
8. X. Zhao and Z.-K. Tan, "Large-area near-infrared perovskite light-emitting diodes," Nat. Photonics **14**(4), 215–218 (2020).
9. X. Gong, Z. Yang, G. Walters, R. Comin, Z. Ning, E. Beauregard, V. Adinolfi, O. Voznyy, and E. H. Sargent, "Highly efficient quantum dot near-infrared light-emitting diodes," Nat. Photonics **10**(4), 253–257 (2016).
10. S. Zhu, B. Shi, and K. M. Lau, "Electrically pumped 1.5 μm InP-based quantum dot microring lasers directly grown on (001) Si," Opt. Lett. **44**(18), 4566–4569 (2019).
11. Z. Jia, C. Yuan, Y. Liu, X.-J. Wang, P. Sun, L. Wang, H. Jiang, and J. Jiang, "Strategies to approach high performance in Cr3+-doped phosphors for high-power NIR-LED light sources," Light: Sci. Appl. **9**(1), 86 (2020).
12. X. Zhang, R. Yi, N. Gagrani, Z. Li, F. Zhang, X. Gan, X. Yao, X. Yuan, N. Wang, J. Zhao, P. Chen, W. Lu, L. Fu, H. H. Tan, and C. Jagadish, "Ultralow threshold, single-mode InGaAs/GaAs multiquantum disk nanowire lasers," ACS Nano **15**(5), 9126–9133 (2021).
13. J. Lu, X. Guan, Y. Li, K. Lin, W. Feng, Y. Zhao, C. Yan, M. Li, Y. Shen, X. Qin, and Z. Wei, "Dendritic CsSnI3 for efficient and flexible near-infrared perovskite light-emitting diodes," Adv. Mater. **33**(44), 2104414 (2021).
14. C. Xie, X. Zhao, E. W. Y. Ong, and Z.-K. Tan, "Transparent near-infrared perovskite light-emitting diodes," Nat. Commun. **11**(1), 4213 (2020).
15. K. T. Ly, R.-W. Chen-Cheng, H.-W. Lin, Y.-J. Shiau, S.-H. Liu, P.-T. Chou, C.-S. Tsao, Y.-C. Huang, and Y. Chi, "Near-infrared organic light-emitting diodes with very high external quantum efficiency and radiance," Nat. Photonics **11**(1), 63–68 (2017).

16. J. Li, N. Gao, D. Cai, W. Lin, K. Huang, S. Li, and J. Kang, “Multiple fields manipulation on nitride material structures in ultraviolet light-emitting diodes,” Light: Sci. Appl. **10**(1), 129 (2021).
17. B. Shi, K. Jie, Y. Zhou, J. Zhou, D. Xia, and F. Huang, “Nanoparticles with near-infrared emission enhanced by pillararene-based molecular recognition in water,” J. Am. Chem. Soc. **138**(1), 80–83 (2016).
18. A. Minotto, I. Bulut, A. G. Rapidis, G. Carnicella, M. Patrini, E. Lunedei, H. L. Anderson, and F. Cacialli, “Towards efficient near-infrared fluorescent organic light-emitting diodes,” Light: Sci. Appl. **10**(1), 18 (2021).
19. Y.-H. Won, O. Cho, T. Kim, D.-Y. Chung, T. Kim, H. Chung, H. Jang, J. Lee, D. Kim, and E. Jang, “Highly efficient and stable InP/ZnSe/ZnS quantum dot light-emitting diodes,” Nature **575**(7784), 634–638 (2019).
20. S. Busatto, M. de Ruiter, J. T. B. H. Jastrzebski, W. Albrecht, V. Pinchetti, S. Brovelli, S. Bals, M.-E. Moret, and C. de Mello Donega, “Luminescent colloidal InSb quantum dots from In situ generated single-source precursor,” ACS Nano **14**(10), 13146–13160 (2020).
21. C.-H. Wu, H.-A. Chen, S.-Y. Lin, and C.-H. Wu, “1.1 μ InAs/GaAs quantum-dot light-emitting transistors grown by molecular beam epitaxy,” Opt. Lett. **40**(16), 3747–3749 (2015).
22. J. Xiong and S.-T. Wu, “Planar liquid crystal polarization optics for augmented reality and virtual reality: from fundamentals to applications,” eLight **1**(1), 3 (2021).
23. F.-L. Wu, S.-L. Ou, Y.-C. Kao, C.-L. Chen, M.-C. Tseng, F.-C. Lu, M.-T. Lin, and R.-H. Horng, “Thin-film vertical-type AlGaInP LEDs fabricated by epitaxial lift-off process via the patterned design of Cu substrate,” Opt. Express **23**(14), 18156–18165 (2015).
24. C.-W. Cheng, K.-T. Shiu, N. Li, S.-J. Han, L. Shi, and D. K. Sadana, “Epitaxial lift-off process for gallium arsenide substrate reuse and flexible electronics,” Nat. Commun. **4**(1), 1577 (2013).
25. X. Zhu, F. Lin, Z. Zhang, X. Chen, H. Huang, D. Wang, J. Tang, X. Fang, D. Fang, J. C. Ho, L. Liao, and Z. Wei, “Enhancing performance of a GaAs/AlGaAs/GaAs nanowire photodetector based on the two-dimensional electron-hole tube structure,” Nano Lett. **20**(4), 2654–2659 (2020).
26. P. Dutta, M. Rathi, D. Khatiwada, S. Sun, Y. Yao, B. Yu, S. Reed, M. Kacharia, J. Martinez, A. P. Litvinchuk, Z. Pasala, S. Pouladi, B. Eslami, J.-H. Ryou, H. Ghasemi, P. Ahrenkiel, S. Hubbard, and V. Selvamanickam, “Flexible GaAs solar cells on roll-to-roll processed epitaxial Ge films on metal foils: a route towards low-cost and high-performance III-V photovoltaics,” Energy Environ. Sci. **12**(2), 756–766 (2019).
27. M. Rashidi, T. Haggren, Z. Su, C. Jagadish, S. Mokkapati, and H. H. Tan, “Managing resonant and nonresonant lasing modes in GaAs nanowire random lasers,” Nano Lett. **21**(9), 3901–3907 (2021).
28. M. Jiang, G. He, H. Chen, Z. Zhang, L. Zheng, C. Shan, D. Shen, and X. Fang, “Wavelength-tunable electroluminescent light sources from individual Ga-Doped ZnO microwires,” Small **13**(19), 1604034 (2017).
29. Z. Sun, M. Jiang, W. Mao, C. Kan, C. Shan, and D. Shen, “Nonequilibrium hot-electron-induced wavelength-tunable incandescent-type light sources,” Photonics Res. **8**(1), 91–102 (2020).
30. B. Nikoobakht, R. P. Hansen, Y. Zong, A. Agrawal, M. Shur, and J. Tersoff, “High-brightness lasing at submicrometer enabled by droop-free fin light-emitting diodes (LEDs),” Sci. Adv. **6**(33), eaba4346 (2020).
31. R. P. Hansen, Y. Zong, A. Agrawal, E. Garratt, R. Beams, J. Tersoff, M. Shur, and B. Nikoobakht, “Chip-Scale Droop-Free Fin light-emitting diodes using facet-selective contacts,” ACS Appl. Mater. Interfaces **13**(37), 44663–44672 (2021).
32. M. Liu, M. Jiang, Y. Liu, K. Tang, D. N. Shi, and C. Kan, “Wavelength-tunable green light sources based on ZnO:Ga Nanowire/p-InGaN heterojunctions,” ACS Appl. Nano Mater. **4**(10), 11168–11179 (2021).
33. M. Jiang, K. Tang, P. Wan, T. Xu, H. Xu, and C. Kan, “A single microwire near-infrared exciton-polariton light-emitting diode,” Nanoscale **13**(3), 1663–1672 (2021).
34. X. Zhou, M. Jiang, J. Wu, M. Liu, C. Kan, and D. Shi, “Electrically driven whispering-gallery-mode microlasers in an n-MgO@ZnO:Ga microwire/p-GaN heterojunction,” Opt. Express **30**(11), 18273–18286 (2022).
35. M. Jiang, P. Wan, K. Tang, M. Liu, and C. Kan, “An electrically driven whispering gallery polariton microlaser,” Nanoscale **13**(10), 5448–5459 (2021).
36. K. Tang, P. Wan, C. Kan, M. Liu, D. Shi, and M. Jiang, “Continuous-wave operation of electrically driven single mode microlaser,” Appl. Phys. Lett. **120**(1), 011105 (2022).
37. C. B. Han, C. He, and X. J. Li, “Near-infrared light emission from a GaN/Si nanoheterostructure array,” Adv. Mater. **23**(41), 4811–4814 (2011).
38. X. Yang, C.-X. Shan, P.-N. Ni, M.-M. Jiang, A.-Q. Chen, H. Zhu, J.-H. Zang, Y.-J. Lu, and D.-Z. Shen, “Electrically driven lasers from van der Waals heterostructures,” Nanoscale **10**(20), 9602–9607 (2018).
39. A. Chen, H. Zhu, Y. Wu, G. Lou, Y. Liang, J. Li, Z. Chen, Y. Ren, X. Gui, S. Wang, and Z. Tang, “Electrically driven single microwire-based heterojuction light-emitting devices,” ACS Photonics **4**(5), 1286–1291 (2017).
40. C. Zhang, J. Zhang, W. Liu, H. Xu, S. Hou, C. Wang, L. Yang, Z. Wang, X. Wang, and Y. Liu, “Enhanced ultraviolet random lasing from Au/MgO/ZnO heterostructure by introducing p-Cu2O hole-injection layer,” ACS Appl. Mater. Interfaces **8**(46), 31485–31490 (2016).
41. C. Zhang, Y. Qiu, W. Liu, H. Xu, L. Yang, C. Wang, and Y. Liu, “Improved near-UV electroluminescence of ZnO nanorod array LEDs by coupling with a graphene plasmon layer,” Nanophotonics **8**(12), 2203–2213 (2019).
42. Y. Liu, M. Jiang, G. He, S. Li, Z. Zhang, B. Li, H. Zhao, C. Shan, and D. Shen, “Wavelength-tunable ultraviolet electroluminescence from Ga-Doped ZnO microwires,” ACS Appl. Mater. Interfaces **9**(46), 40743–40751 (2017).

Optics EXPRESS

43. X. Zhou, M. Jiang, Y. Wu, K. Ma, Y. Liu, P. Wan, C. Kan, and D. Shi, "Hybrid quadrupole plasmon induced spectrally pure ultraviolet emission from a single AgNPs@ZnO:Ga microwire based heterojunction diode," Nanoscale Adv. **2**(3), 1340–1351 (2020).
44. W. Liu, Z. Li, Z. Shi, R. Wang, Y. Zhu, and C. Xu, "Nano-buffer controlled electron tunneling to regulate heterojunctional interface emission," Opto-Electron. Adv. **4**(9), 200064 (2021).
45. Z. Li, W. Liu, R. Wang, F. Chen, J. Chen, Y. Zhu, Z. Shi, and C. Xu, "Interface design for electrically pumped ultraviolet nanolaser from single ZnO-nanorod," Nano Energy **93**, 106832 (2022).
46. C. Xu, J. Dai, G. Zhu, G. Zhu, Y. Lin, J. Li, and Z. Shi, "Whispering-gallery mode lasing in ZnO microcavities," Laser Photonics Rev. **8**(4), 469–494 (2014).
47. G. Wu, W. Li, C. Shen, F. Gao, H. Liang, H. Wang, L. Song, and G. Du, "Near infrared electroluminescence from n-InN/p-GaN light-emitting diodes," Appl. Phys. Lett. **100**(10), 103504 (2012).
48. H. Zhu, C.-X. Shan, B. Yao, B.-H. Li, J.-Y. Zhang, Z.-Z. Zhang, D.-X. Zhao, D.-Z. Shen, X.-W. Fan, Y.-M. Lu, and Z.-K. Tang, "Ultralow-threshold laser realized in Zinc Oxide," Adv. Mater. **21**(16), 1613–1617 (2009).
49. D. You, C. Xu, F. Qin, Z. Zhu, A. G. Manohari, W. Xu, J. Zhao, and W. Liu, "Interface control for pure ultraviolet electroluminescence from nano-ZnO-based heterojunction devices," Sci. Bull. **63**(1), 38–45 (2018).
50. A. P. Abiyasa, S. F. Yu, S. P. Lau, E. S. P. Leong, and H. Y. Yang, "Enhancement of ultraviolet lasing from Ag-coated highly disordered ZnO films by surface-plasmon resonance," Appl. Phys. Lett. **90**(23), 231106 (2007).
51. H. Li, J. Tang, F. Lin, D. Wang, D. Fang, X. Fang, W. Liu, R. Chen, and Z. Wei, "Improved optical property and lasing of ZnO nanowires by Ar plasma treatment," Nanoscale Res. Lett. **14**(1), 312 (2019).
52. C. Kan, Y. Wu, J. Xu, P. Wan, and M. Jiang, "Plasmon-enhanced strong exciton-polariton coupling in single microwire-based heterojunction light-emitting diodes," Opt. Express **29**(2), 1023–1036 (2021).
53. S.-H. Lee, S. W. Lee, T. Oh, S. H. Petrosko, C. A. Mirkin, and J.-W. Jang, "Direct observation of plasmon-induced interfacial charge separation in metal/semiconductor hybrid nanostructures by measuring surface potentials," Nano Lett. **18**(1), 109–116 (2018).
54. A. Pescaglini, A. Martin, D. Cammi, G. Juska, C. Ronning, E. Pelucchi, and D. Iacopino, "Hot-electron injection in Au Nanorod-ZnO Nanowire hybrid device for near-infrared photodetection," Nano Lett. **14**(11), 6202–6209 (2014).
55. L. J. Brillson and Y. Lu, "ZnO Schottky barriers and Ohmic contacts," J. Appl. Phys. **109**(12), 121301 (2011).